ASSESSMENT OF TOMOGRAPHIC PIV USING EXPERIMENTAL AND DNS DATA IN TURBULENT CHANNEL FLOWS

Charitha M. de Silva[1*]**, Rio Baidya**[1] **and Ivan Marusic**[1]

1: Department of Mechanical Engineering
University of Melbourne, Victoria 3010, AUSTRALIA.
*corresponding author: c.desilva3@pgrad.unimelb.edu.au

Abstract   In this paper we study the influence of experimental parameters such as camera positioning in three-dimensional space, seeding density, interrogation volume size and spatial resolution on tomographic particle image velocimetry (Tomo-PIV) measurements in turbulent channel flows. To perform this, Tomo-PIV simulations are carried out that employ camera modelling, a Mie scattering illumination model, lens distortion effects and a calibration model. Further analysis of Tomo-PIV is performed by conducting experiments in a channel flow facility, with matched flow characteristics to the direct numerical simulation (DNS) data used in the simulation study.

1. Introduction

The ability to accurately measure three-dimensional information and associated structures of turbulent flows is of great interest, as it helps to reveal the topology of turbulent flows. Three-dimensional three-component (3D-3C) velocity measurements techniques have become increasingly available over the past decade, particularly in the area of particle image velocimetry. These techniques include holographic PIV (HPIV) (Barnhart et al., 1994), 3D scanning PIV (Brücker, 1996), defocusing PIV (Willert and Gharib, 1992), 3D particle tracking velocimetry (PTV) (Maas et al., 2004), synthetic aperture PIV (SAPIV) (Belden et al., 2010) and tomographic-PIV (Tomo-PIV) (Elsinga et al., 2006).

This paper focuses on Tomo-PIV (Elsinga et al., 2006) which is based on a tomographic reconstruction of an intensity field representing a volume from multiple view points. The studies performed in this paper provide an insight into the achievable accuracy in Tomo-PIV measurements performed on wall-bounded flows. An analysis is performed to optimise several experimental parameters such as camera positioning, seeding density, and the interrogation volume size, which relates directly to the spatial averaging of the measurement. Studies performed by Hutchins et al. (2009) showed that the senor length in hotwire anemometry can have a significant impact on the attenuation of the flow statistics. Similarly in PIV, averaging is performed across the interrogation window or volume (Saikrishnan et al., 2006). In the case of Tomo-PIV a three dimensional averaging is performed in comparisons to the 2D and 1D averaging in planar PIV and hotwire anemometry respectively. Therefore, Tomo-PIV can produce significantly attenuated flow statistics especially in the near wall region that are associated with high velocity gradients in the wall-normal direction.

1.1 Simulation study

The accuracy of Tomo-PIV is predominantly driven by image quality and the algorithms used for reconstruction and cross-correlation. In addition to these parameters, the accuracy of Tomo-PIV is also influenced by several experimental parameters which are analysed in this simulation study. The novelty of the simulation study presented herein is the application of channel flow DNS data at Re_τ = 934 (del Alamo et al., 2004) to displace the synthetic particles, providing a realistic vector flow field for a wall-bounded turbulent flow with a large wall-normal heterogeneity. In comparison, Worth et al. (2010) performed a resolution study on Tomo-PIV based on homogenous isotropic turbulence DNS data. Other studies presented by Lecordier and Westerweel (2008) used a constant displacement for all particles. Further details on the methodology of the simulation study used here can be found in de Silva et al. (2012).

Throughout this paper we use the coordinate system x, y and z to refer to the streamwise, spanwise and wall-normal directions with corresponding velocity components given by U, V and W. The fluctuating velocity components are denoted by the corresponding lower case letters (u, v and w). The superscript + refers to normalisation with the viscous inner scale. For example, $l^+ = lU_\tau/\nu$ and $U^+ = U/U_\tau$, where U_τ is the friction velocity and ν is the kinematic viscosity of the fluid. Furthermore, we use the angle brackets $\langle\rangle$ to denote volumetric averaging across many wall positions, and overbars (‾) to indicate spatial averaging at a single wall-normal position.

Results presented in this simulation study include an analysis on camera position and orientation in three-dimensional space to obtain an optimal reconstruction quality for a given Tomo-PIV experiment. Previous studies performed by Elsinga et al. (2006) have documented the effect of adjusting the angle between the laser sheet and the camera position by projecting 1D images onto a 2D array of pixels. Here, we aim to simulate the effect of moving each camera in three-dimensional space by adjusting the camera's azimuthal (θ) and elevation (ϕ) angles as shown in figure 1(a). In addition, the simulations are performed by projecting 2D images onto a 3D volume, which enables us to obtain a realistic estimate of the achievable reconstruction quality in a typical Tomo-PIV experiment. The simulations also model typical lighting used in a Tomo-PIV experiment enabling us to analyse the effect of forward and backward scatter in relation to the direction of illumination. Furthermore, we analyse the effectiveness of Tomo-PIV to resolve turbulent statistics in wall-bounded turbulent flows. This is performed by a quantitative comparison of flow statistics obtained at various voxel discretisation levels to DNS channel flow statistics. This enables us to determine the voxel discretisation level necessary to obtain flow statistics to within a certain accuracy in wall-bounded turbulence. In addition, a ratio relating the number of particles and the interrogation volume size is proposed based on the accuracy of flow statistics, which can be used to determine the optimum seeding density (de Silva et al., 2012).

1.2 Experimental Study

The applicability of the results observed for camera positioning, seeding density, interrogation volume size and spatial resolution in the simulation study is verified by analysis of a data set from a Tomo-PIV experiment. Since it is practically infeasible to run several experiments at each camera position and spatial resolution, the experiment is configured for the optimal values determined during the simulation study. In addition, the experiment is performed at a matched Reynolds number to the DNS data used in the simulation study (Re_τ = 934). This enables us to obtain a realistic assessment of the attainable accuracy in a Tomo-PIV experiment for wall-bounded turbulent flows, and report on its limitations for this application. Comparisons are also drawn on the flow statistics obtained from the experimental data and spatially averaged DNS flow statistics. This set of averaged statistics is obtained by applying a three-dimensional mean filter over several DNS flow fields till a converged set of statistics is obtained. The filter size is set to match the interrogation volume size used to process the Tomo-PIV data. This enables us to determine how accurately a 3D box filter can model the attenuation observed in a typical Tomo-PIV experiment.

2. Results and discussion

2.1 Camera position and orientation

To analyse the effect of moving each camera in the 3D space we adjust each camera's azimuthal and elevation angles as shown in figure 1(a). To increase the feasibility of the analysis only four camera configurations are considered. Each camera is positioned using a spherical coordinate system based on the angles θ and ϕ and a constant radial distance of 5000^+ (5000 inner viscous length units) from the centre of the reconstructed volume located at (x, y, $z = 0$). To enable a quantitative comparison of the reconstruction

quality the reconstruction quality Q is determined using

$$Q = \frac{\sum_{x,y,z} E_1(x,y,z).E_0(x,y,z)}{\sqrt{\sum_{x,y,z} E_1^2(x,y,z).\sum_{x,y,z} E_0^2(x,y,z)}} \qquad (1)$$

where $E_1(x,y,z)$ is the reconstructed intensity field, and $E_0(x,y,z)$ is an ideal reconstruction intensity field based on known particle positions (Elsinga et al., 2006). The angles θ and ϕ are varied from $5° - 85°$ and $20° - 85°$ respectively, to determine the achievable quality factor Q at each position. It should be noted that, elevation angles below $20°$ are not considered since the reconstructed volume is highly skewed to the camera position. In addition, a Scheimpflug adapter will not be able to align the focal plane of the camera and the mid-plane of the synthetic volume in such cases (de Silva et al., 2012). In this analysis we consider a forward scatter, backward scatter and a camera configuration with all cameras placed on a single side of the laser sheet.

2.1.1 Camera configuration with all cameras placed on a single side of the laser sheet

This is the most commonly used configuration (shown in figure 1(a)) since it is usually easier to setup and calibrate. Figure 1(b) shows the variation of Q at each camera position and orientation. It should be noted that here we present results for a single camera since the four cameras are placed and moved while maintaining symmetry. These results are then normalised by the maximum attainable Q (Q_{max}) obtained from a polynomial fit for the given configuration. Results presented in figure 2 indicate that within the range of $50° < \phi < 60°$ and $20° < \theta < 25°$, a Q greater than 95% of Q_{max} is obtained. A further deviation of $\pm 5°$ reduces Q to 90% of Q_{max}, after which a rapid reduction in reconstruction quality is observed (de Silva et al., 2012).

(a) Camera configuration

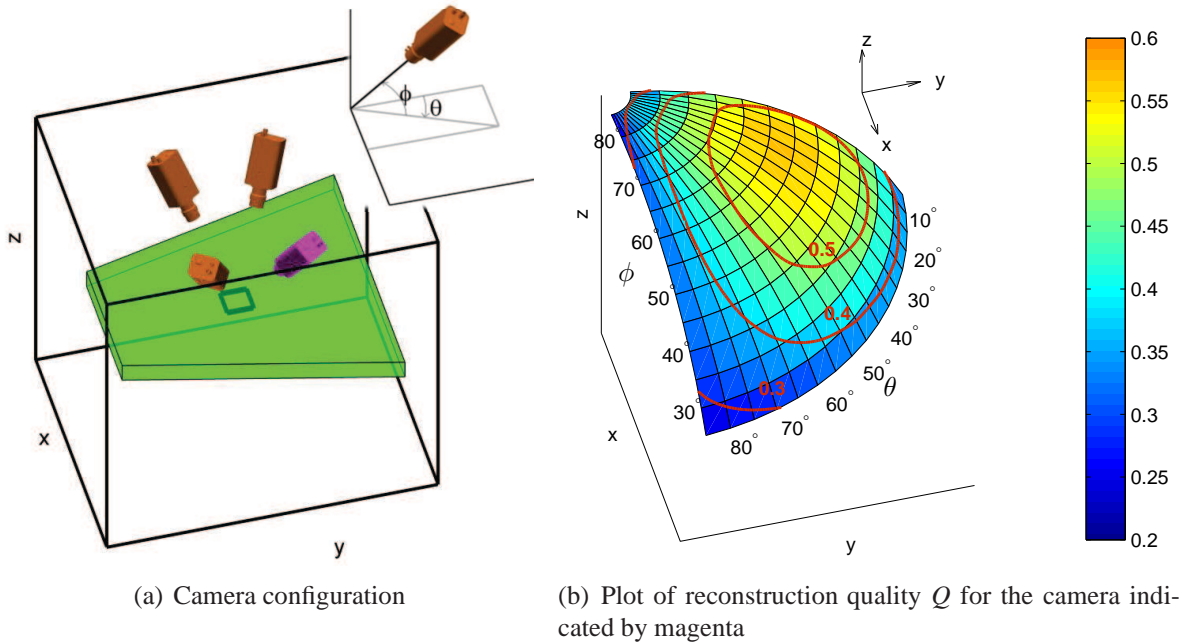(b) Plot of reconstruction quality Q for the camera indicated by magenta

Figure 1: All cameras placed on a single side of laser. (de Silva et al., 2012)

A comparison to previous studies performed using 2D simulations by Elsinga et al. (2006) is shown in figure 3, together with results obtained from this study at $\theta = 25°$. This enables a comparison between the optimal elevation angle between the two studies. Figure 3 indicates a similarity in the trend observed for Q at varying θ, however it should be noted that the magnitude of Q obtained from this study is less than that observed by Elsinga et al. (2006). This is expected as the simulations performed here are three dimensional which results in a fundamental drop in reconstruction quality as demonstrated by Elsinga et al. (2006). In addition, we model a calibration procedure, image distortion, Mie scattering and camera noise
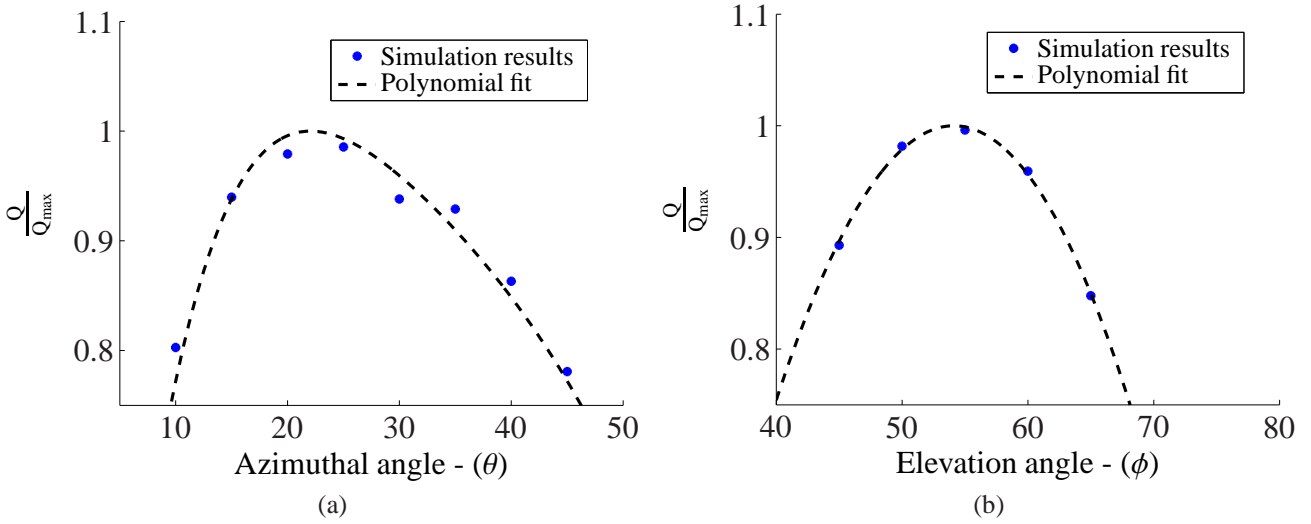
Figure 2: Plot of reconstruction quality Q/Q_{max} at (a) the optimal elevation ($\phi = 55°$) for varying azimuthal angles (θ) and (b) the optimal azimuthal angle ($\theta = 25°$) at varying elevation angles (ϕ). (de Silva et al., 2012)

which lead to a further drop in Q. However we believe our simulations provides a better representation of the reconstruction quality observed in Tomo-PIV experiments.

2.1.2 Alternate Configurations

Simulations are also run for forward and backward scatter configurations where all cameras are placed in either forward or backward scatter in relation to the direction of the laser sheet. Figure 4 shows a two-dimensional slice at $\phi = 55°$ for the variation in reconstruction quality with θ. The results show a consistently higher Q for the forward scatter configuration. This is expected since the seeding particles scatter more light in the forward scatter direction (Bohren and Huffman, 1983) which is accounted for in the Mie scatter model used in the simulations. An extensive analysis on these configurations can be found in de Silva et al. (2012).
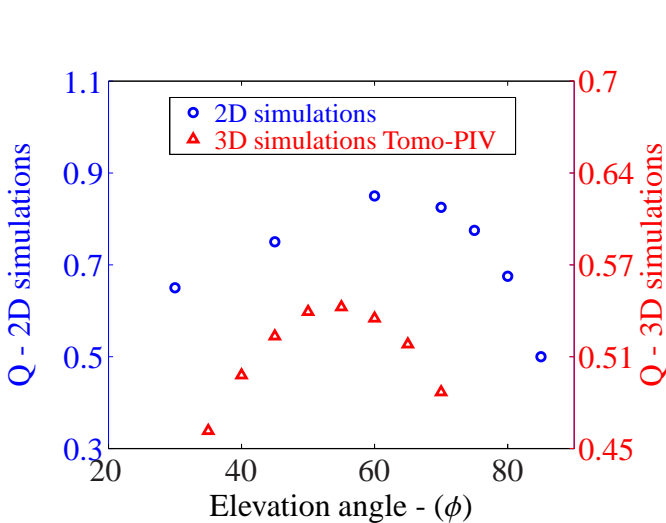

Figure 3: Comparison between 2D simulations results obtained by Elsinga et al. (2006) and the Tomo-PIV simulation results at $\theta = 25°$. (de Silva et al., 2012)
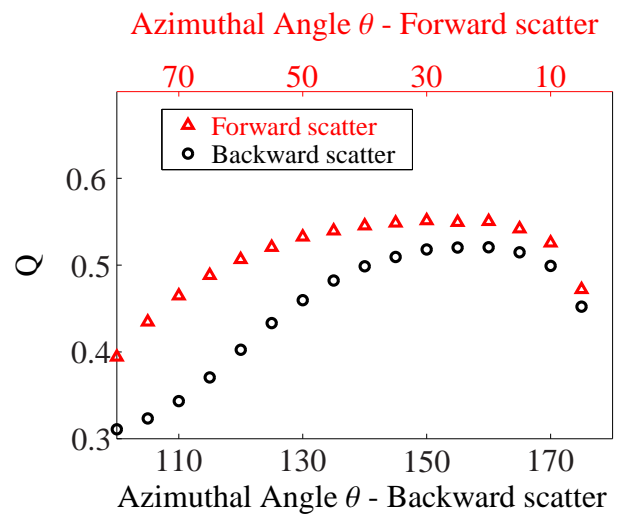
Figure 4: Comparison of reconstruction quality between forward and backward scatter at $\phi = 55°$ for varying azimuthal angles (θ). (de Silva et al., 2012)

2.2 Volume discretisation (Voxel Size)

As noted previously, flow statistics from wall-bounded flows can be attenuated by spatial averaging, particularly in the near wall-region. Here, we aim to determine the effect of the voxel discretisation level while maintaining other parameters constant, which include a constant interrogation volume length of $l^+ = 20$. Further details on the setup of the simulations can be found in de Silva et al. (2012). To visualise the accuracy at varying volume discretisation levels, a comparison of the flow statistics $\langle U \rangle^+$, $\langle u^2 \rangle^+$, $\langle v^2 \rangle^+$ and $\langle w^2 \rangle^+$ is made between the simulation results and the original DNS results. This comparison is performed against the original DNS statistics obtained from del Alamo et al. (2004) and DNS statistics averaged over the same interrogation volume positions of each simulation (averaged DNS statistics). This enables us to eliminate the attenuation due to spatial averaging across the interrogation volume, thereby, isolating the variation in accuracy due to the voxel discretisation level.

Table 1 summarises the results obtained, as expected an increase in accuracy is obtained at a higher spatial resolution, particularity in the second order statistics. However, this improvement in accuracy is diminishing as the spatial resolution is increased further. This is evident in figure 5 where the accuracy increases linearly with l_v^+ on a logarithmic scale. It can be seen that a discretisation level of $l_v^+ = 0.63$ is sufficient to obtain an error less than 3% in the second order statistics compared to the averaged DNS statistics, which we consider within a acceptable range for experimental error. Although increasing the spatial resolution further improves accuracy, this improvement does not outweigh the disadvantages associated with an increased spatial resolution. This includes using a higher resolution camera which is more expensive and tends to have lower frame rates. Similarly, lenses which provide a smaller l_v^+ have a reduced field of view due to increased magnification.

Voxel size (l_v^+)	0.94	0.63	0.47
Tomo-PIV simulation vs. averaged DNS statistics	%	%	%
$\langle U \rangle^+$	0.43	0.17	0.08
$\langle u^2 \rangle^+$	3.99	1.47	0.44
$\langle v^2 \rangle^+$	7.42	1.55	1.05
$\langle w^2 \rangle^+$	7.53	2.41	1.10
Tomo-PIV simulation vs. DNS statistics	%	%	%
$\langle U \rangle^+$	0.95	0.65	0.09
$\langle u^2 \rangle^+$	4.68	3.62	2.06
$\langle v^2 \rangle^+$	11.22	5.59	5.06
$\langle w^2 \rangle^+$	12.69	7.57	6.40

Table 1: Summary of percentage errors for flow statistics in the region $100 < z^+ < 200$ with an interrogation volume length of $l^+ = 20$. (de Silva et al., 2012)
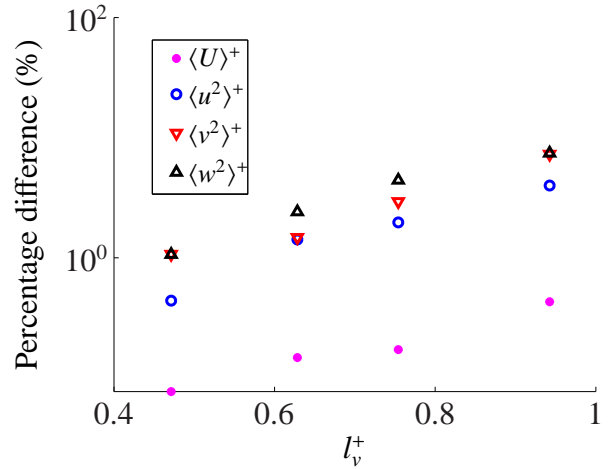

Figure 5: Accuracy for varying voxel sizes for statistics in the region $100 < z^+ < 200$ with an interrogation volume length of $l^+ = 20$, compared to averaged DNS statistics. (de Silva et al., 2012)

2.3 Particles per interrogation volume (N_I) & Seeding Density

Here we investigate the influence of the seeding density by varying the number of synthetic particles and the interrogation volume size while keeping the other parameters constant. Similar to the study presented in § 2.2 a quantitative comparison is made between simulation and DNS flow statistics at varying (N_I) with a fixed interrogation volume size (de Silva et al., 2012). These results indicate that the optimal N_I varies with interrogation volume size. Therefore, we propose a ratio between N_I and the interrogation volume size, S_d, which is calculated using

$$S_d = \frac{N_I}{I_x I_y I_z}, \tag{2}$$

where I_x, I_y, I_z are the interrogation volume sizes in voxels in the x, y, z directions respectively. Figure 6 presents results for varying interrogation volume sizes for the parameter S_d. It is evident that $S_d \approx 1.4 \times 10^{-4}$ provides the optimal accuracy that remains consistent across the interrogation volume sizes considered. Therefore, we propose that this value can be used as a reference to determine the required seeding density. It should be noted that, to use this parameter it is necessary to reconstruct a single frame to approximate N_I and determine the current value of S_d.
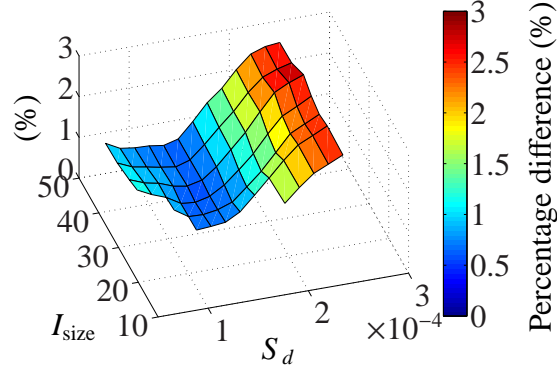

Figure 6: Comparison between simulation results and averaged DNS statistics for $\langle u^2 \rangle^+$ in the region $100 < z^+ < 200$ for varying seeding density (S_d) and interrogation volume size ($I_{\text{size}} = I_x, I_y, I_z$). (de Silva et al., 2012)

2.4 Experimental Investigation

An experimental investigation is performed to match the optimal experimental parameters determined using the simulation study. This enables us to validate the accuracy of the simulation study by a quantitative comparison against the experimental data. In addition, we can obtain a realistic assessment of the attainable accuracy in a Tomo-PIV experiment for wall-bounded turbulent flows, enabling us to report on its limitations for this application. The tomographic imaging system consists of four PCO4000 cameras (4008×2672 pixels, 2Hz) equipped with 105mm Nikon lenses. The above setup enables us to obtain a reconstructed volume size of $\approx 1.5\delta \times 1\delta \times 0.2\delta$, where δ denotes the half-channel height of 0.05m. The cameras are positioned and orientated to within 90% of the optimum azimuthal ($\theta \approx 23°$) and elevation ($\phi \approx 55°$) angles (de Silva et al., 2012). It should be noted, that a frontal mirror is used to reflect the laser light to improve illumination for the given camera configuration as shown in figure 7. The images are processed using an in-house Tomo-PIV package, details of the algorithms used are given in de Silva et al. (2012). A pixel to voxel ratio of 1 is maintained in the reconstruction giving a volume size of $4008 \times 2672 \times 534$ voxels. In addition, the cross-correlation is performed with an interrogation volume length of l^+15 with a corresponding voxel characteristic length of $l_v^+ \approx 0.41$.

The experiments are conducted in the channel flow facility at the Walter Bassett Aerodynamics Laboratory located at the University of Melbourne. Details of the construction of the channel flow facility are provided in Monty (2005). Table 2 summarises the flow conditions and the key parameters of the Tomo-PIV experiment.

To visualise the accuracy of the experimental results, flow statistics $\overline{U}^+$, $\overline{u^2}^+$, $\overline{v^2}^+$ and $\overline{w^2}^+$ are presented in figure 8. Each sub-figure consists of the experimental results and DNS statistics (del Alamo et al., 2004). In addition an averaged set of DNS statistics is included to enable us to compare the accuracy of the technique, neglecting the attenuation caused by the interrogation volume size. It should be noted that, although the near-wall region ($z^+ < 50$) is imaged, due to issues such as reflections from the wall a reliable vector field is not obtainable in this region. Results in figure 8 suggests that the Tomo-PIV is resolving the flow statistics well, with good agreement between the averaged DNS statistics and the experimental results. To further validate this agreement, a comparison is made at a larger interrogation volume size. Results at an interrogation volume length of $l^+ = 30$ are presented in figure 9. Although the experimental results
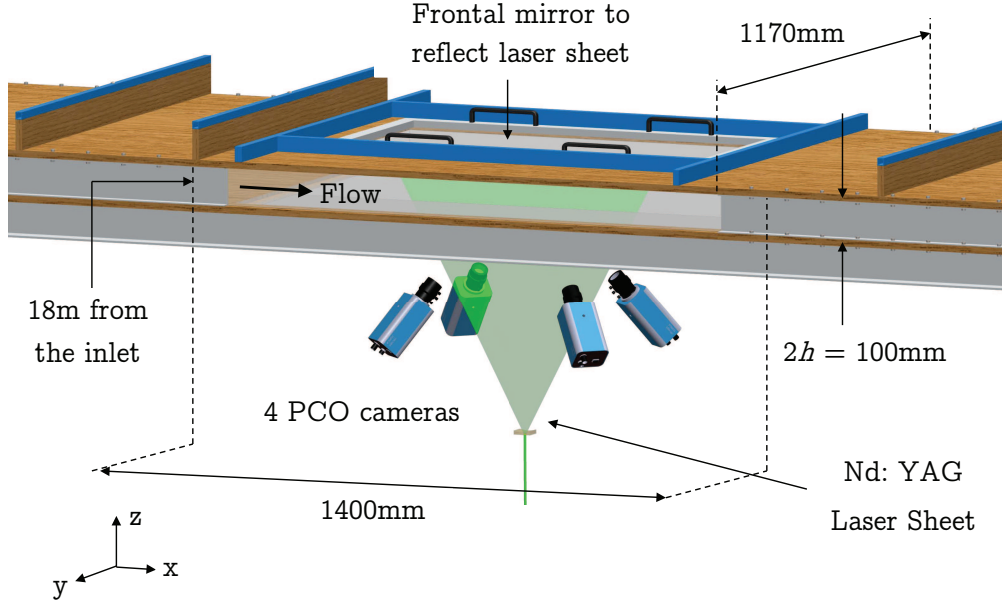
Figure 7: Experimental setup for Tomo-PIV in channel flow.

Table 2: Summary of experiment and processing parameters for Tomo-PIV experiment

Re_τ	936
U_τ	0.292 m/s
ν	$1.56 \times 10^{-5} \mathrm{m}^2/\mathrm{s}$
Number of cameras	4
Sample rate	2Hz
Laser sheet thickness	10mm
Voxel size l_v^+	≈ 0.41
Reconstruction volume size	$\approx 1.5\delta \times 1\delta \times 0.2\delta$
Reconstruction volume size (voxels)	$4008 \times 2672 \times 534$
Number of volumes reconstructed	1000
Cubic interrogation volume size l^+	≈ 15
Reconstruction algorithm	MLOS based in-house technique (de Silva et al., 2012) which uses a 3$^{\mathrm{rd}}$ order polynomial calibration fit and a bi-cubic interpolation scheme to determine the voxel intensities to sub-pixel accuracy.
Cross-correlation algorithm	Template matching scheme based on Lewis (1995) which incorporates several advancements discussed in Scarano (2001).

are heavily attenuated in comparison to the DNS statistics it is in good agreement with the averaged DNS statistics. Therefore, we can conclude that the expected attenuation of the flow statistics from a typical Tomo-PIV can be predicted from applying a 3D box filter to several DNS fields. A similar observation is likely to be seen in planar PIV although not analysed in this paper. However, in the case of planar PIV it is important to account for the laser sheet thickness, which needs to be determined accurately to provide a realistic three-dimensional filter size to avoid underestimating the attenuation.

A summary of the accuracy in first and second order statistics between the experimental, DNS data and averaged DNS data is given in table 3. These results are obtained from the region $100 < z^+ < 200$ with an interrogation volume length of $l^+ = 15$. A comparison to the simulation results in table 1 obtained at a similar voxel discretisation level indicates that the simulations provide a good estimate on the achievable accuracy. As expected, the experimental results show a higher error. This is primarily because the simulations are idealistic in comparison to an actual experiment, which is affected by fixed

Table 3: Summary of absolute percentage errors for flow statistics in the region $100 < z^+ < 200$ with an interrogation volume length of $l^+ = 15$

	Experimental Tomo-PIV vs. averaged DNS statistics (%)	Experimental Tomo-PIV vs. DNS statistics (%)
$\langle U \rangle^+$	0.17	0.17
$\langle u^2 \rangle^+$	0.80	2.28
$\langle v^2 \rangle^+$	1.06	1.83
$\langle w^2 \rangle^+$	4.68	8.05

pattern noise, lens aberrations, foreign objects, reflections and calibration errors.

Based on previous Tomo-PIV literature we would expect the velocity component corresponding to the direction of the laser sheet thickness (spanwise in this experiment) to be least accurate. This is caused by limitations of Tomo-PIV, which include a Gaussian shaped laser sheet intensity and poor reconstruction quality in depth. However, the results show the largest discrepancies in the wall-normal turbulence intensity and the Reynolds shear stress at both interrogation volume sizes considered. We believe this is primarily caused by the smaller turbulence intensity of the wall-normal velocity component in comparison to the spanwise and streamwise components. This leads to a lower voxel displacement usually in the sub-pixel regime, which hinders the accuracy of the cross-correlation phase. It should be noted that, most techniques used to perform multi-component measurements in wall-bounded flows have lower accuracy in the wall-normal velocity component for reasons mentioned previously.

Since we obtain instantaneous spatial multi-component velocity data we are able to calculate vorticity statistics. In the case of Tomo-PIV we are able to determine all three components of the vorticity in the streamwise, spanwise and wall-normal directions. This information is considered to be very valuable in the scientific community for this type of flow as most measurement techniques are unable to provide a 3D-3C measurement. Figures 10(a) and 10(b) shows the mean $(\overline{\Omega_y}^+)$ and variance $(\overline{\omega_y^2}^+)$ of the spanwise vorticity respectively together with the original DNS and averaged DNS statistics. The results indicate a good match in the mean statistics and a reasonable approximation of the variance is given by the averaged DNS statistics. It should be noted that, the accuracy of the vorticity is affected by velocity gradients, hence we expect the results to be more susceptible to measurement noise. This can be observed in the near wall-region and at the edges of the reconstructed volume on figure 10(b). Similar results are seen for the variance $\overline{\omega_x^2}^+$ and $\overline{\omega_z^2}^+$, which are not shown here.

Figure 11 shows the one-dimensional pre-multiplied streamwise energy spectra as a function of the streamwise wavenumber (k_x^+) at selected wall positions. Such a comparison is useful since they readily show the energy scales present at various wavenumbers for a given wall-normal location. One should note that the primary purpose of this comparison is to quantitatively asses the ability of a Tomo-PIV measurement to resolve the energy scales present in a wall-bounded turbulent flow within a given field of view. Here, we are limited to $k_x^+ > 0.0042$ which corresponds to the wavenumber of the instantaneous streamwise field of view. In addition, the interrogation volume length and the overlap dictates the largest wavenumber that can be resolved. Here we use $l^+ = 15$ with 50% overlap, and therefore we are limited to $k_x^+ < 0.41$. A close match is observed between the averaged DNS statistics and the experimental results beyond $z^+ > 200$, however prior to this a clear attenuation can be observed in the experimental results which exceed the predicted attenuation from spatially averaged DNS data especially at a interrogation volume length of $l^+ = 15$. This can be attributed to experimental error associated with the measurement especially in the near-wall region ($z^+ < 50$) to reasons detailed previously. This discrepancy is reduced when considering a larger interrogation volume length as shown in figure 11(b), we believe this is due to the increased accuracy in the cross-correlation with a larger interrogation volume size. In addition, we observe an increase in the spectrogram at large wave numbers ($k_x^+ > 0.10$) in the near wall region. This is primarily caused due to the measurement noise present in the velocity field obtained from the Tomo-PIV
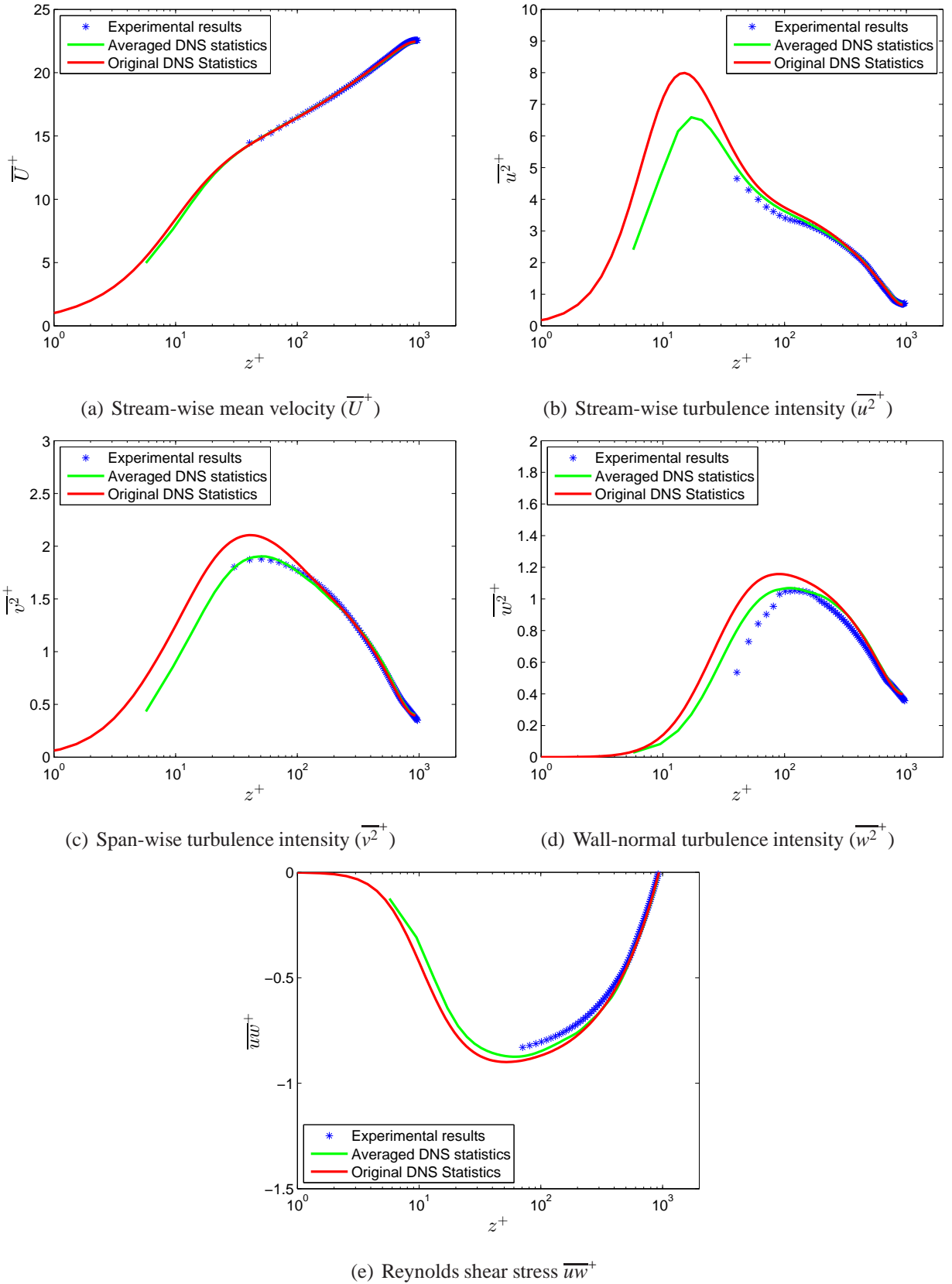
(a) Stream-wise mean velocity ($\overline{U}^+$)

(b) Stream-wise turbulence intensity ($\overline{u^2}^+$)

(c) Span-wise turbulence intensity ($\overline{v^2}^+$)

(d) Wall-normal turbulence intensity ($\overline{w^2}^+$)

(e) Reynolds shear stress $\overline{uw}^+$

Figure 8: Comparison of experimental results and DNS statistics for flow statistics $\overline{U}^+$, $\overline{u^2}^+$, $\overline{v^2}^+$, $\overline{w^2}^+$ and $\overline{uw}^+$ with an interrogation volume length of $l^+ = 15$.

measurement. Based on theses results, it is expected that in the near wall region the energy spectra cannot be relied upon for an accurate map of the energy scales present in the flow. Similar results are also seen
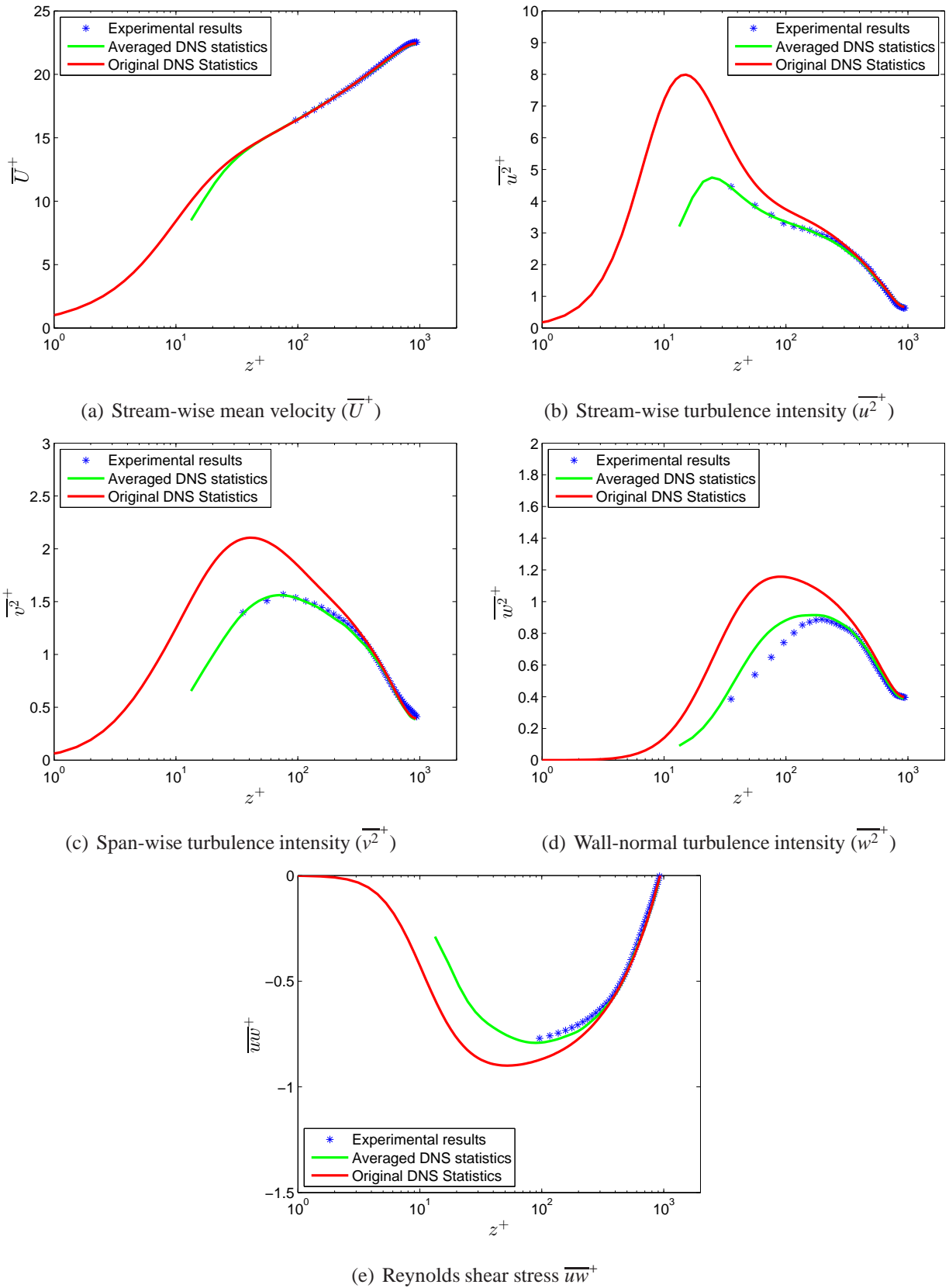
(a) Stream-wise mean velocity ($\overline{U}^+$)

(b) Stream-wise turbulence intensity ($\overline{u^2}^+$)

(c) Span-wise turbulence intensity ($\overline{v^2}^+$)

(d) Wall-normal turbulence intensity ($\overline{w^2}^+$)

(e) Reynolds shear stress $\overline{uw}^+$

Figure 9: Comparison of experimental results and DNS statistics for flow statistics $\overline{U}^+$, $\overline{u^2}^+$, $\overline{v^2}^+$, $\overline{w^2}^+$ and $\overline{uw}^+$ with an interrogation volume length of $l^+ = 30$.

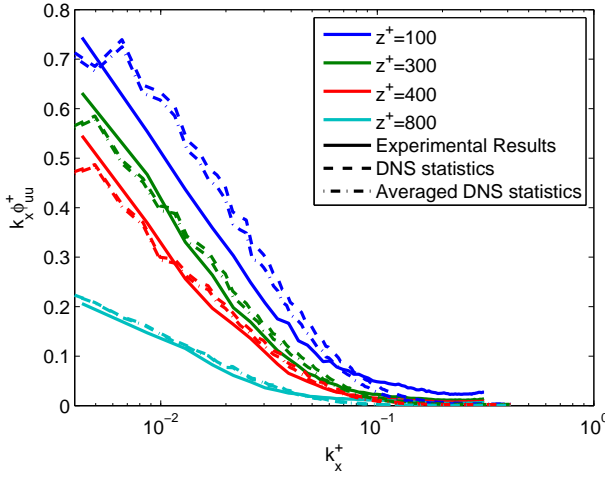for the pre-multiplied spanwise and wall-normal energy spectra as a function of k_x^+, which are not shown here.
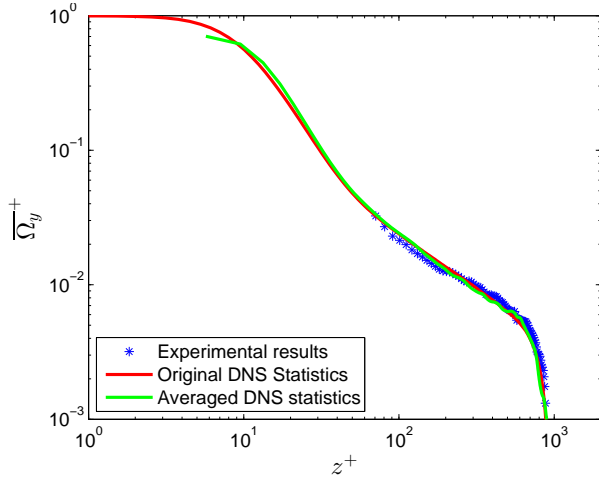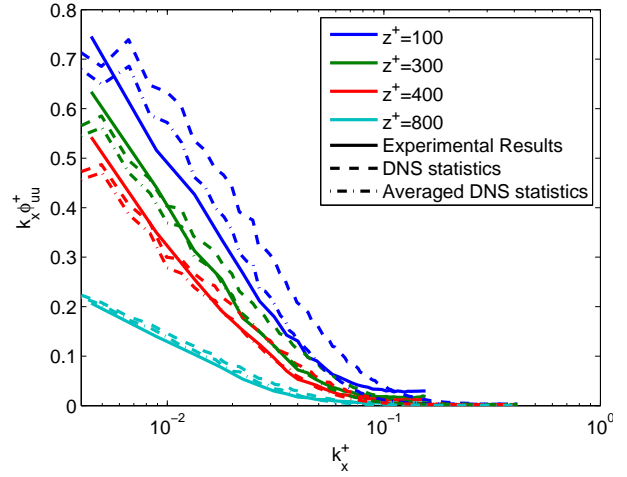
(a) Mean spanwise vorticity ($\overline{\Omega_y}^+$)
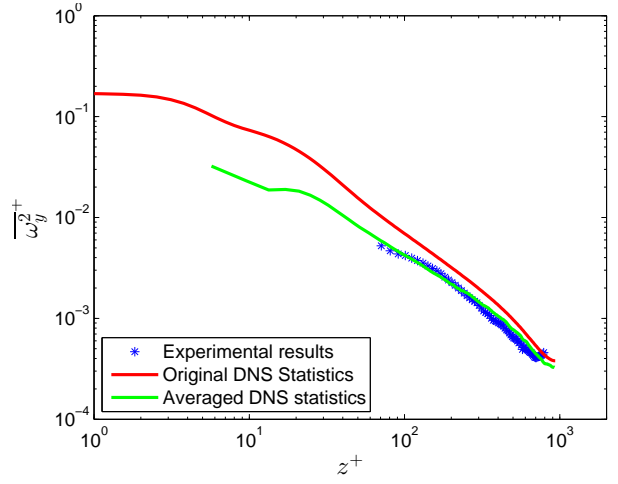
(b) Variance of spanwise vorticity ($\overline{\omega_y^2}^+$)

Figure 10: Comparison of experimental results and DNS statistics for flow statistics $\overline{\Omega_y}^+$ and $\overline{\omega_y^2}^+$ with an interrogation volume length of $l^+ = 15$.

(a) Interrogation volume length of $l^+ = 15$

(b) Interrogation volume length of $l^+ = 30$

Figure 11: Comparison of Experimental results and DNS statistics for the pre-multiplied one-dimensional streamwise energy spectra $k_x \phi_{uu}^+$ at various wall normal locations.

3. Conclusion

A quantitative assessment on the application of Tomo-PIV in wall-bounded turbulence with particular reference to turbulent channels flows is presented here. A summary of the study performed in de Silva et al. (2012) on the influence of several experimental parameters such as camera positioning, seeding density and voxel discretisation is reviewed and extended here by comparison to experimental data obtained at matched flow conditions. A comparison between experimental and simulation results suggest that the simulation study is indicative of the attainable accuracy in a typical Tomo-PIV experiment on wall-bounded flows. Flow statistics obtained from the experimental data shows that Tomo-PIV is capable of measuring first and second order flow statistics to within 0.1% and 5% of the averaged DNS statistics at a interrogation volume size of $l^+ = 15$. This error reduces as the interrogation volume size is increased however the statistics are heavily attenuated in comparison to the original DNS statistics (del Alamo et al., 2004) due to spatial filtering.

In this study we observe that a good indication of the expected attenuation for flow statistics in a typical Tomo-PIV experiment is given by the averaged DNS statistics, where the averaging is performed across the interrogation volume size. Although this comparison is performed at matched flow conditions, studies performed by Hutchins and Marusic (2007) have shown that in the case of boundary layer flows as Reynolds number increases only the large scale energy changes, and the attenuation observed in this study is predominantly restricted to the viscous scale with wavenumbers above $k_x^+ \sim O(0.01)$. Furthermore, studies performed by Monty et al. (2009) shows that near viscous energy is nominally equivalent between channel, pipe and boundary layer flows. Therefore, we believe that the attenuation predicted by the averaged DNS statistics applies to Tomo-PIV measurements in wall-bounded flows for a range of Reynolds numbers. This implies that a correction scheme can be formulated by calculating the difference between the averaged and original DNS statistics which can be used to correct flow statistics from Tomo-PIV measurements in wall-bounded flows. It should be noted, that this analogy can be extended to other variants of PIV such as planar PIV.

References

Barnhart, D. H., Adrian, R. J., and Papen, G. C. Phase-conjugate holographic system for high-resolution particle-image velocimetry. *Appl. Opt.*, 33(30):7159–7170, 1994.

Belden, J., Truscott, T., Axiak, M., and Techet, A. Three-dimensional synthetic aperture particle image velocimetry. *Meas Sci Technol*, 21(12):125403, 2010.

Bohren, C. and Huffman, D. *Absorption and scattering of light by small particles*. John Wiley & Sons Inc., New York, 1983.

Brücker, C. 3D scanning-particle-image-velocimetry: Technique and application to a spherical cap wake flow. *Appl Sci Res*, 56:157–179, 1996.

de Silva, C. M., Baidya, R., Khashehchi, M., and Marusic, I. Assessment of tomographic PIV in wall-bounded turbulence using direct numerical simulation data. *Exp Fluids*, 52(2):425–440, 2012.

del Alamo, J., Jimenez, J., Zandonade, P., and Moser, R. Scaling of the energy spectra of turbulent channels. *J Fluid Mech*, 500:135–144, 2004.

Elsinga, G., Scarano, F., Wieneke, B., and van Oudheusden, B. Tomographic particle image velocimetry. *Exp Fluids*, 41: 933–947, 2006.

Hutchins, N. and Marusic, I. Evidence of very long meandering features in the logarithmic region of turbulent boundary layers. *J Fluid Mech*, 579:1–28, 2007.

Hutchins, N., Nickels, T., Marusic, I., and Chong, M. Hot-wire spatial resolution issues in wall-bounded turbulence. *J Fluid Mech*, 635:103–136, 2009.

Lecordier, B. and Westerweel, J. The EUROPIV synthetic image generator. Technical report, 2008.

Lewis, J. Fast normalized cross-correlation. *Vision Interface*, 1995.

Maas, H., Gruen, A., and Papantoniou, D. Particle tracking velocimetry in three-dimensional flows. *Exp Fluids*, 15: 133–146, 2004.

Monty, J. *Developments in smooth wall turbulent duct flows*. PhD thesis, The University of Melbourne, 2005.

Monty, J. P., Hutchins, N., Ng, H., Marusic, I., and Chong, M. A comparison of turbulent pipe, channel and boundary layer flows. *J Fluid Mech*, 632:431–442, 2009.

Saikrishnan, N., Marusic, I., and Longmire, E. K. Assessment of dual plane PIV measurements in wall turbulence using DNS data. *Exp Fluids*, 41:265–278, 2006.

Scarano, F. Iterative image deformation methods in PIV. *Meas Sci Technol*, 13:R1–19, 2001.

Willert, C. E. and Gharib, C. E. Three-dimensional particle imaging with a single camera. *Exp Fluids*, 12:353–358, 1992.

Worth, N., Nickels, T., and Swaminathan, N. A tomographic PIV resolution study based on homogeneous isotropic turbulence DNS data. *Exp Fluids*, 49:637–656, 2010.